



## COB-2021-0060

# TAKEOFF SPEEDS DETERMINATION USING A MULTIDISCIPLINARY OPTIMIZATION TOOL

### Carolina Barbosa Coimbra

Embraer Commercial Aviation - Av. Brigadeiro Faria Lima, 2170 - Putim, São José dos Campos - SP  
carolina.coimbra@embraer.com.br / carolinabcoimbra@gmail.com

### Vinícius Leite de Moraes Véras

Embraer Commercial Aviation - Av. Brigadeiro Faria Lima, 2170 - Putim, São José dos Campos - SP  
vinicius.veras@embraer.com.br / viniciuslmveras@gmail.com

**Abstract.** This paper presents a tool that implements an optimization process to determine the takeoff speed schedule of a commercial jet in compliance with CFR-14 Part-25 regulation. The goal was, assuming one-engine inoperative (OEI), to determine the rotation speed ( $V_R$ ) that minimizes the error between the  $V_{35}$  - as predicted by a dynamic simulation of a complete 6DoF aircraft model - and the target speed at 35ft screen height ( $V_2$ ). An optimization workflow was developed using modeFRONTIER, which connects the aircraft model implemented in Simulink with scripts in MATLAB and Python. Analyses were performed for different weights, center of gravity positions, runway heights, temperatures, and  $V_2/V_S$  ratios with the engine failure assumed at minimum ground control speed ( $V_{MCG}$ ). Maneuver margins and minimum unstick speed constraints were implemented in the workflow. Once the  $V_R$  was determined in OEI condition, it was used to simulate all engines operating (AEO) takeoff. Speed and time increments for the rotation to liftoff (RO-LO) and the liftoff to screen height (LO-SH) segments were obtained. The curves of  $V_R$ ,  $V_{LOF}$ , and  $V_2$  normalized by the stall speed ( $V_S$ ) were also obtained as a function of the climb gradient, as a mean for visually determine the configurations for which the performance can be improved and what the limiting factors may be.

**Keywords:** takeoff, speed schedule, optimization, performance.

## 1. INTRODUCTION

Takeoff is one of the most critical flight phases since the aircraft is close to the ground, at low speed, heavy weight, and low energy, what makes it difficult to correct eventual piloting mistakes or react to external disturbances. In order to assure safety, takeoff performance determination is regulated for commercial aircraft by CFR 14 (FAA, 2021) and RBAC (ANAC, 2014) in §25.105 and §25.107. The requirements for takeoff speeds ( $V_R$ ,  $V_{LOF}$  and  $V_2$ ), are defined in §25.107. Those speeds are illustrated in Fig. 1 and although §25.113 defines that the takeoff run is equal to the takeoff distance if there is no clearway, in this figure they are represented separately once the performance textbooks usually divide the takeoff procedure into ground and air phases for modeling purposes (Raymer, 1989) (Anderson, 2010).

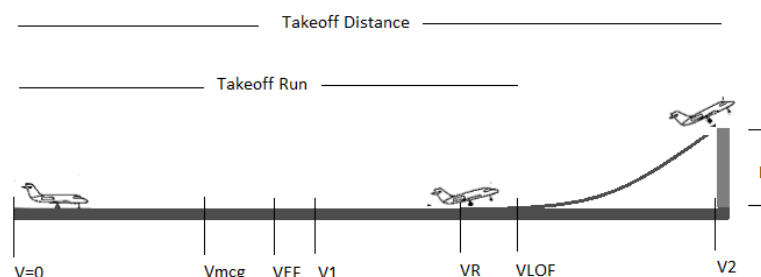


Figure 1. Takeoff Speeds at One-engine Inoperative Condition

The problem of takeoff speeds determination is essentially an inverse problem in the sense that typically a selected safety speed ( $V_2$ ) is given. Then, assuming that  $V_2$  is reached at 35ft with one-engine inoperative, a performance model is used to compute the liftoff ( $V_{LOF}$ ) and rotation ( $V_R$ ) speeds that lead to  $V_2$  at 35ft. As per §25.107(e)(2), a single  $V_R$  must be used for both one-engine inoperative (OEI) and all engines operating (AEO) conditions. Thus, the performance model can be used assuming AEO condition to obtain  $V_{LOF}$  and  $V_{35}$  (airspeed at 35ft for AEO condition).

The Advisory Circular AC25-7D (FAA, 2018) provides, at section 4.2, guidance for flight test evaluations to determine

the takeoff speeds at different conditions of weight, altitude and temperature within the operational limits of the aircraft in compliance with CFR 14 Part 25.

This paper presents an automated process of obtaining the takeoff speeds and corresponding takeoff performance within a simulation environment in order to have an accurate estimate of the aircraft performance before the start of a flight test campaign, hence reducing development time and cost (Donateo *et al.*, 2018), (Gemma and Mastroddi, 2019), (de Mattos *et al.*, 2018).

## 2. METHODOLOGY

### 2.1 PROBLEM DEFINITION

To determine the aircraft takeoff speed schedule and takeoff performance the rotation speed ( $V_R$ ) must be determined at one-engine inoperative (OEI) condition for different climb gradients and  $V_2/V_S$  ratios. The  $V_R$  calculations are iterated until the calibrated speed at 35ft - output of the simulation model - equals the takeoff safety speed ( $V_2$ ) - simulation input obtained from the  $V_2/V_S$  ratio. The optimization problem can be defined as follows:

**Objective Function:** To minimize the difference between the calibrated airspeed at 35ft and the selected  $V_2$  (Eq. (1)).

**Optimization Variable:** Rotation speed ( $V_R$ ), which was limited between  $V_2 - 15\text{kt}$  and  $V_2 - 1\text{kt}$ .

**Design Points:** The optimization was performed at four different weights, three center of gravity positions and three different altitudes and temperatures - relative to the International Standard Atmosphere (ISA) - within the operational envelope of the aircraft, as shown in Tab. 1. Engine failure speed was assumed constant at minimum ground control speed ( $V_{MCG}$ ) and  $V_2/V_S$  ratio was set between 1.15 and 1.20 with a step of 0.01.

**Constraints:** To assure the solution results on a certifiable performance, two constraints were considered during optimization: the maneuver margin and the ratio between the liftoff speed ( $V_{LOF}$ ) and the minimum unstick speed ( $V_{MU}$ ) according to §25.107(d) (FAA, 2021).

$$\begin{cases} J = (f_{V35}(V_R) - V_2)^2 \\ V_R^* = \text{argmin} \{J(V_R)\} \end{cases} \quad (1)$$

Table 1. Boundaries of Design Variables

Variable	Lower Boundary	Upper Boundary	Number of points
Rotation speed ( $V_R$ )	$V_2 - 15\text{kt}$	$V_2 - 1\text{kt}$	12
Weight	Min. Operating Weight (MOW)	Max. Takeoff Weight (MTOW)	4
Center of Gravity (CG)	Forward CG	Aft CG	3
Runway Altitude	Sea Level	4000 ft	3
Temperature	ISA + 0°C	ISA + 35°C	3
$V_2/V_S$ ratio	1.15	1.20	6

### 2.2 OPTIMIZATION WORKFLOW

The optimization workflow was developed using modeFRONTIER (modeFRONTIER, 2018) as an integration platform, which connects the complete six degrees of freedom flight dynamics model of the aircraft in Simulink, shown at Fig 2, with simulation scripts in Matlab (MATLAB, 2012) and post processing scripts in Python (Van Rossum and Drake Jr., 2009).

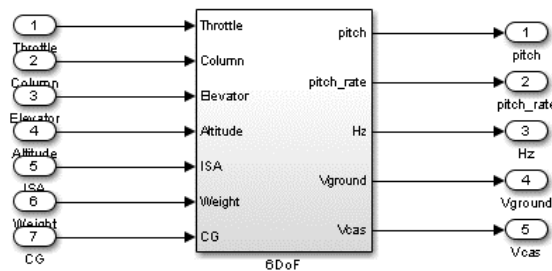


Figure 2. Complete 6 Degrees of Freedom Flight Dynamics Model of the Aircraft in Simulink

The scripts were integrated to the workflow using modeFRONTIER MATLAB and Python calling blocks.

Since the rotation speed ( $V_R$ ) must be determined assuming OEI for different climb gradients, the optimization was divided into two workflows, connected with a "scheduling project" block. The inner workflow (Fig. 3) was responsible for the iterative process of determining the  $V_R$  for which the speed at 35 ft equals the reference V2 at OEI condition. The outer one (Fig. 4) was responsible for setting different values for the design point variables and utilizing the results of inner workflow to determine the performance in AEO condition.

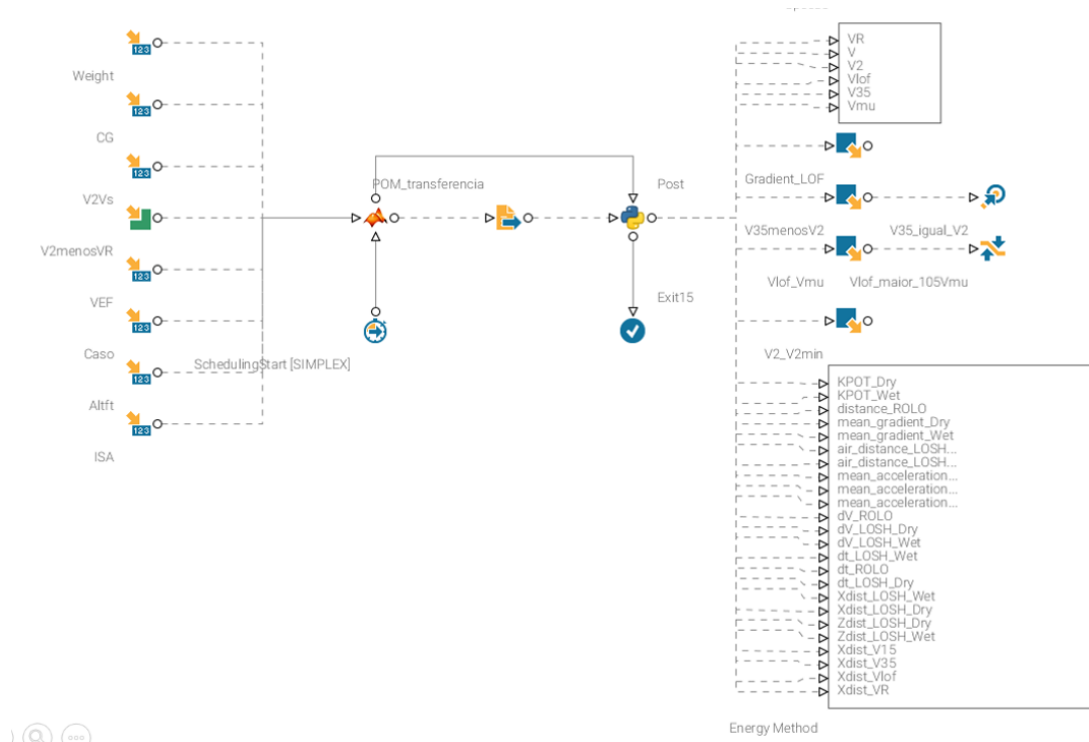


Figure 3. Rotation Speed Optimization Workflow

In order to simplify the implementation of the optimization workflow, it was implemented in such a way that the minimizing argument was  $\Delta V_{RO-SH} = V2 - V_R$ . As V2 was defined in terms of stall speed ( $V2 = kV_S$ ), stall speed was calculated in MATLAB for each takeoff weight and then utilized to determine the reference V2. This value was then subtracted with the speed increment from rotation ( $V_R$ ) to V2 to determine the reference rotation speed ( $V_R = V2 - \Delta V_{RO-SH}$ ). After the simulation, it is necessary to select the output variables important for takeoff performance using a post-processing script, which was implemented in Python.

The post-processing script was based on the energy method (Anderson, 2010) and the simulation model outputs were utilized to determine takeoff events and the respective speed and position relative to the runway headland. The output variables were, finally, connected to objective and constraint blocks for the optimization.

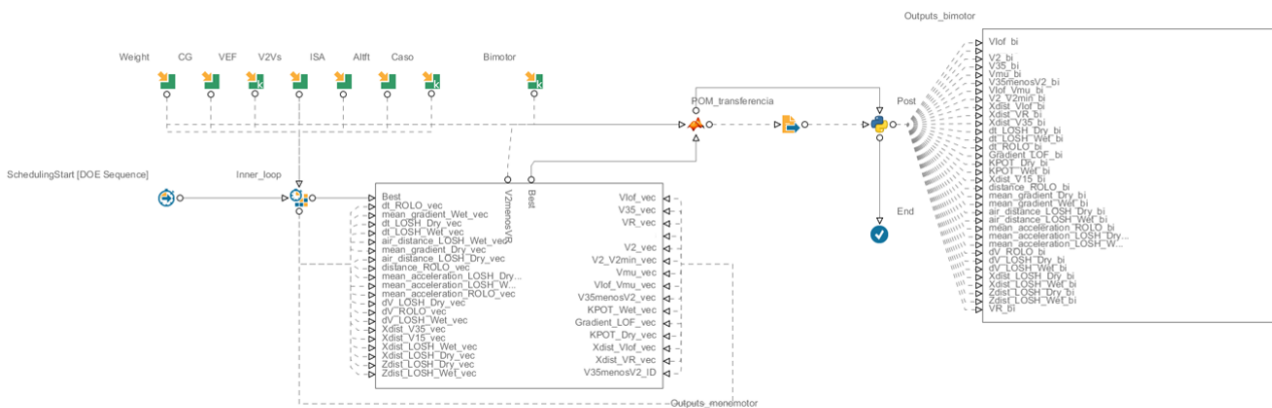


Figure 4. Takeoff Condition Setting Workflow

The rotation speed that produced the minimum error between V35 and V2 at OEI condition was identified in the outer workflow, shown at Fig. 4, and utilized as input for AEO simulation.

### 2.3 OPTIMIZATION ALGORITHM

Once the workflow was build in modeFRONTIER a series of tests were conducted to determine which optimization algorithm could find a rotation speed ( $V_R$ ) with a V35 minus V2 lower than 0.1 knots and with minimum computational effort. Three algorithms were tested: MOGA II genetic algorithm (Poles, 2003a), SimpleX heuristic algorithm (Poles, 2003b) (Goldbarg, 2005), and B-BFGS gradient based algorithm (Rigone, 2003). Each optimization was evaluated considering a total of 60 simulations. Then, the best solution encountered for each algorithm and the overall optimization time were compared.

Table 2 shows the results obtained for each optimization algorithm. Clearly MOGA II is faster than the other two, however the minimum error between the speed at 35 ft at OEI condition and the reference V2 is 4 times higher and the number of takeoff conditions optimized simultaneously is lower. This is explained by the fact that MOGA II requires more simulation points to convergence and, during the tests, the number of total simulations poits was limited to 60. Hence, MOGA II was tested for only two takeoff conditions with 30 iterations each, while SimpleX and B-BFGS were tested for five takeoff conditions with 12 iterations each. As for SimpleX and B-BFGS results, the heuristic algorithm was 20% faster and both minimum error between V35 and V2 stayed below the goal of 0.1 knots.

Table 2. Optimization Algorithm Performance Comparison

Algorithm	Takeoff Conditions Optimized	Optimization Time	Min Error  V35-V2
MOGA II	2	1.5h	0.29kt
SimpleX	5	2h	0.07kt
B-BFGS	5	2.5h	0.06kt

Therefore, SimpleX was chosen to be the optimization algorithm of the inner workflow. For each climb gradient, the number of simulation points was limited to 12 and a stop condition was set for  $|V35-V2| \leq 0.1$  kt. In each run 4 takeoff conditions are optimized simultaneously and repeated points are not simulated again.

## 3. RESULTS AND DISCUSSION

### 3.1 LIMITING FACTORS

To understand what the limiting factors for improving the aircraft performance were, a series of simulations were executed for one specific takeoff condition. In those simulations, the engine failure speed was kept constant at  $V_{MCG}$  and, for each  $V2/V_S$  ratio defined at Tab. 1, the rotation speed was chosen from V2 - 1kt to V2 - 10kt. The results are presented in Fig. 5 where  $V_{Si}$  is a stall speed based on an arbitrary value of  $CL_{max}$ .

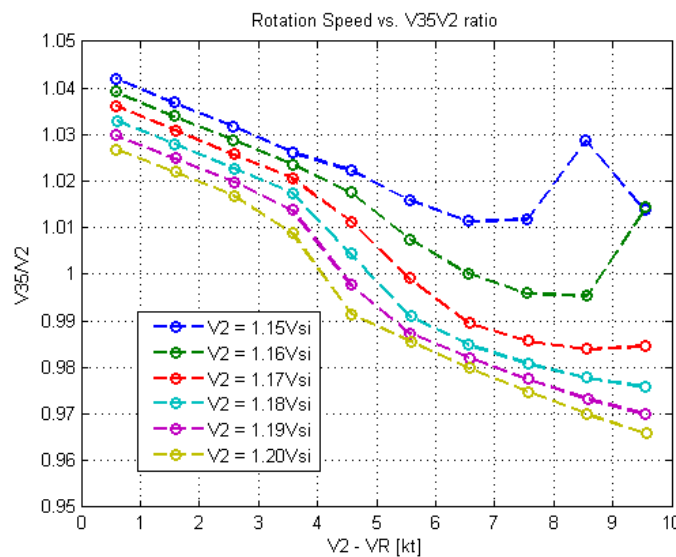


Figure 5. Rotation Speed Distance to V35 vs.  $V35/V2$  ratio at One-engine Inoperative Condition

The figure shows that the higher the safety speed ( $V2$ ), the lower must be the difference between V35 and the rotation

speed ( $V_R$ ) for a given takeoff condition. This was expected once the aircraft needs more kinetic energy to get to the same altitude at the end of the runway (35 ft screen height), at a higher  $V_2$ . It is also clear that there is a limit of  $V_2/V_S$  ratio for which it is possible to determine the rotation speed that turns  $V_{35}/V_2$  ratio equals to one. For the commercial aircraft tested, this limit is of  $V_2 = 1.16 * V_{Si}$ , as shown by dark blue and green curves, for the condition evaluated. Lastly, it shows that the range of optimal  $V_R$  is within 4 to 7 knots below the desired  $V_2$ .

To better visualize how the rotation and safety speed influence the takeoff distance and consequently the required runway length, a three-dimensional plot was generated by adding a third axis to Fig. 5. Figure 6 shows the result. In this figure, it is possible to see that the takeoff distance is reduced by lowering the rotation speed if the  $V_2/V_S$  ratio is higher than 1.17. For lower values of  $V_2/V_S$ , however, non-linear effects were observed at lower  $V_R$  due to  $CL$  insufficiency.

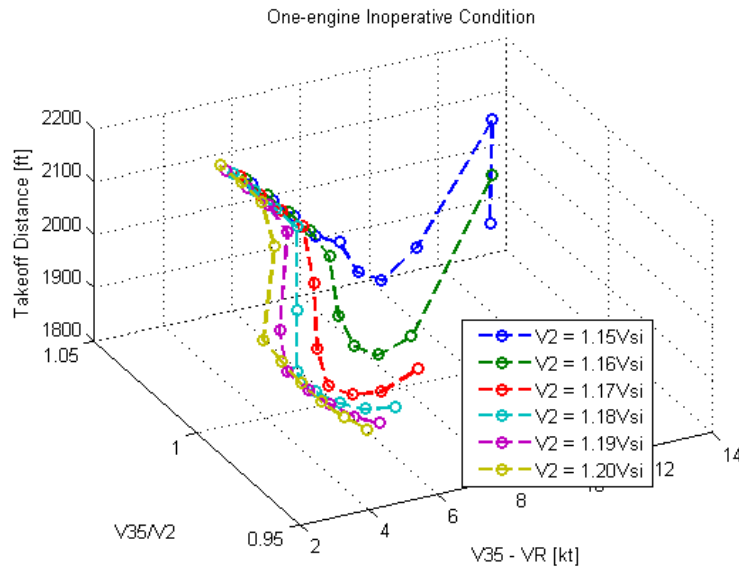


Figure 6. Influence of  $V_R$  and  $V_2$  at Takeoff Distance

This result demonstrates the importance of carefully determining the aircraft's speed schedule once the required takeoff distance can be a limiting factor for short runways such as London City (LCY) and Santos Dumont (SDU) airports. By reducing the  $V_2/V_S$  ratio and the rotation speed so that  $V_{35}/V_2$  ratio is equal to one, the takeoff distance can be reduced, improving the aircraft performance in such airports, thus generates more value for the airlines.

However, a few limiting factors must be taking into consideration while choosing the  $V_2/V_S$  ratio. The first one is the  $V_{LOF}/V_{MU}$  ratio, which, according with CFR 14 Part 25 (FAA, 2021), must be greater than 1.05 for OEI condition and 1.10 for AEO condition. The second limiting factor is the minimum takeoff safety speed ( $V_{2MIN}$ ) as per §25.107(b) (FAA, 2021) required for keeping the maneuver margin.

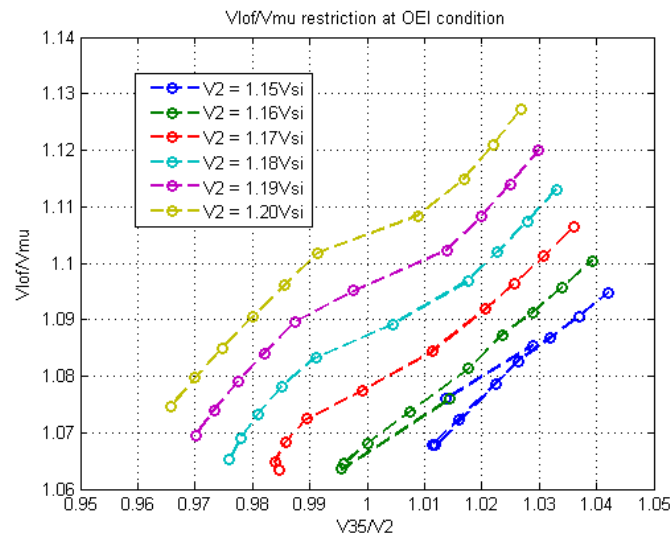


Figure 7.  $V_{LOF}/V_{MU}$  restriction at One-engine inoperative condition vs.  $V_{35}/V_2$  ratio

To understand how  $V_{LOF}/V_{MU}$  restriction may affect the results, Fig. 7 shows the relations between  $V_{LOF}/V_{MU}$  ratio and the  $V_{35}/V_2$  ratio. In order to simplify the analysis the simulation liftoff speed was assumed equal to the  $V_{LOF}$  at maximum practicable rotation rate maneuver. The figure shows that for this particular takeoff condition the restriction of  $V_{LOF}/V_{MU} < 1.05$  was not reached and therefore all values of  $V_2/V_S$  could be considered valid. The maneuver margin, however, typically limits the  $V_2/V_S$  ratio to 1.16 or 1.17.

### 3.2 SPEED AND TIME INCREMENTS

Once the limiting factors were understood, the optimization was set for the conditions defined at Tab. 1 using a Full Factorial Design of Experiments (DOE). The results were then analyzed in terms of speed and time increments for each segment as a function of mean acceleration between  $V_R$  and  $V_{LOF}$  and of center of gravity position, which are presented in Fig. 8 and Fig. 9.

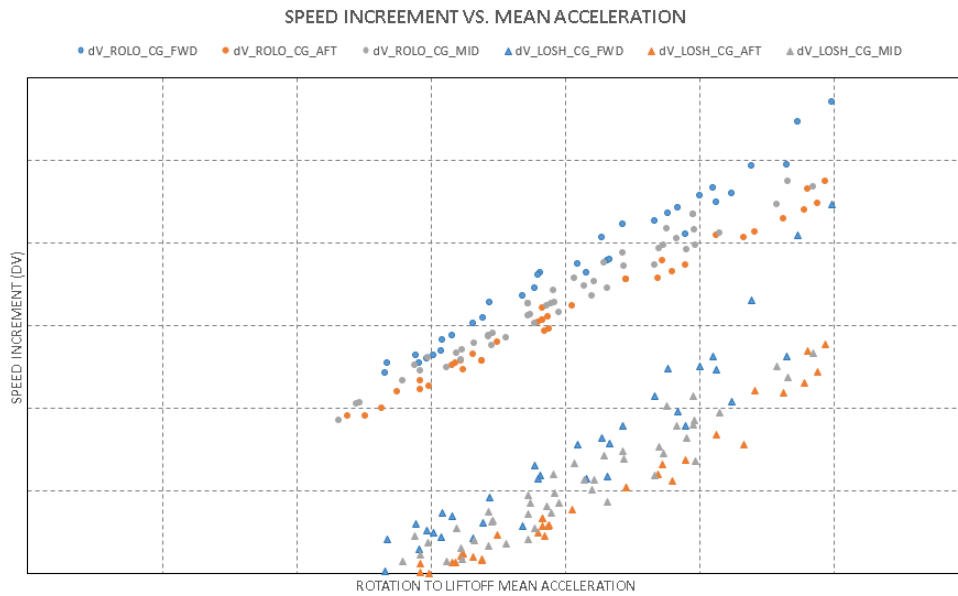


Figure 8. Speed Increments per Segment vs. Mean Acceleration at RO-LO

Figure 8 shows that the relation between the speed increment and the acceleration is approximately linear and that the increment is higher at RO-LO segment followed by LO-SH segment. This result was expected as in the air segments the energy is utilized for both climbing and gaining speed and in the ground segment it is used only for gaining speed.

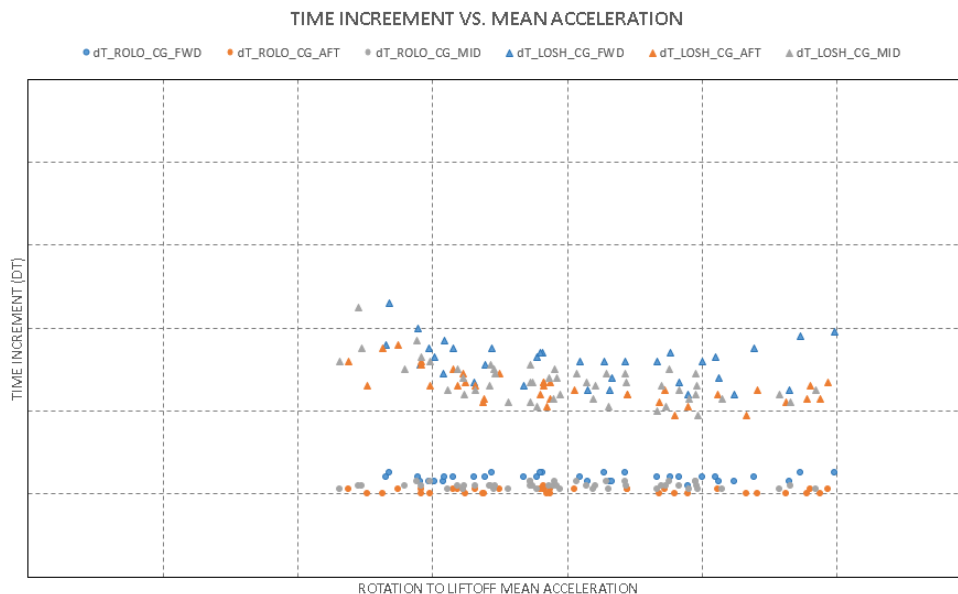


Figure 9. Time Increment vs. Mean Acceleration at RO-LO

Figure 9, on the other hand, shows that the time increment of each segment is approximately constant. The results are the opposite of speed increment, showing that more time was spent at LO-SH than at RO-LO segment.

In both figures the speed and time increments of RO-LO and LO-SH segments were higher for the forward CG configuration, which increases the required takeoff distance. This results corroborates the AC25-7D requirements showing that the critical condition is the FWD CG and, therefore, the flight tests must be conducted on it.

Those results are important for analyzing the aircraft's takeoff performance once they demonstrate how the energy is transformed from kinetic to potential and how each segment contributes for the total takeoff distance. The results were also compared with flight test data showing the workflow has a good accuracy to predict the aircraft's takeoff performance.

#### 4. CONCLUSION

This work allowed Embraer to fully explore the performance potential of products already in the market, generating additional value for clients and potentially creating new demands. It also works as a proof-of-concept, as it is by itself a use case of modeFRONTIER in an innovative way to solve complex problems in a multidisciplinary approach, providing accurate results with reduced development time and cost.

The model developed in this work indicates that forward CG positions have the effect of increasing takeoff distances, which is an important aspect raised by AC25-7D and explicit in some of the CFR 14 Part 25 requirements. It was also possible to evaluate the behavior of the takeoff distance as a function of rotation speed  $V_R$  and safety speed ( $V_2$ ), as well as the correlations between those speeds and time lapses from rotation to screen height (35ft).

This work focused on takeoff performance and takeoff speeds determination, however the optimization workflow could be reproduced for different flight phases, aircraft models or objectives which increases the gain potential of this tool for Embraer.

#### 5. ACKNOWLEDGEMENTS

The authors would like to thank EMBRAER S.A. for the support during the preparation of this work.

#### 6. REFERENCES

- ANAC, 2014. "Regulamento brasileiro de aviação civil nº 25 - requisitos de aeronavegabilidade: Avioes categoria transporte". Agência Nacional de Aviação Civil, Available at: <<https://www.anac.gov.br/assuntos/legislacao/legislacao-1/boletim-de-pessoal/2009/16s/rbac-25-2013-22-04-2009>>. Accessed 23 april 2021.
- Anderson, J.D., 2010. *Aircraft Performance and Design*. Tata McGraw-Hill.
- de Mattos, B.S., Komatsu, P.J. and Tomita, J.T., 2018. "Optimal wingtip device design for transport airplane". Vol. 90, pp. 743–763. doi:<https://doi.org/10.1108/AEAT-07-2015-0183>.
- Donateo, T., Ficarella, A. and Spedicato, L., 2018. "A method to analyze and optimize hybrid electric architectures applied to unmanned aerial vehicles". Vol. 90, pp. 828–842. doi:<https://doi.org/10.1108/AEAT-11-2016-0202>.
- FAA, 2018. "Advisory circular: Flight test guide for certification of transport category airplanes". Federal Aviation Administration, Available at: <<https://www.faa.gov>>. Accessed 26 april 2021.
- FAA, 2021. "Airworthiness standard: Transport category airplanes". Federal Aviation Administration, Available at: <<https://www.ecfr.gov/cgi-bin/text-idx?node=14:1.0.1.3.11>>. Accessed 16 april 2021.
- Gemma, S. and Mastroddi, F., 2019. "Multi-disciplinary and multi-objective optimization of an over-wing-nacelle aircraft concept". Vol. 10, pp. 771–793. doi:<https://doi.org/10.1108/AEAT-07-2015-0183>.
- Goldbarg, M.C., 2005. *Otimização Combinatória e Programação Linear: Modelos e Algoritmos*. ELSEVIER, Rio de Janeiro.
- MATLAB, 2012. "version r2012b". The MathWorks Inc. Natick, Massachusetts.
- modeFRONTIER, 2018. "version 2018r2". ESTECO. Trieste, Italy.
- Poles, S., 2003a. "Moga-ii: An improved multi-objective genetic algorithm". Technical Report 2003-006, ESTECO, Trieste, Italy.
- Poles, S., 2003b. "The simplex method". Technical Report 2003-005, ESTECO, Trieste, Italy.
- Raymer, D.P., 1989. *Aircraft Design: A Conceptual Approach*. AIAA Education Series.
- Rigone, E., 2003. "Bounded bfgs". Technical Report 2003-007, ESTECO, Trieste, Italy.
- Van Rossum, G. and Drake Jr., F.L., 2009. *Python 3 Reference Manual*. CreateSpace, Scotts Valley, CA.

#### 7. RESPONSIBILITY NOTICE

The authors are solely responsible for the printed material included in this paper.